Advanced Functional Materials

ADVANCED FUNCTIONAL MATERIALS
www.afm-journal.de

RESEARCH ARTICLE OPEN ACCESS

Hot-Film and Calorimetric Methods With Transient Heating for Measurement of High Biofluid Flow Rate

Yuanting Wei[1] | Shupeng Li[1] | Kyung Rok Pyun[2] | Tianyu Yang[3] | Bosung Kim[2] | Haotian Yang[1] | John A. Rogers[2,4,5,6,7] | Yonggang Huang[1,2,4,5] | Haohui Zhang[1]

[1]Department of Civil and Environmental Engineering, Northwestern University, Evanston, Illinois, USA | [2]Querrey Simpson Institute For Bioelectronics, Northwestern University, Evanston, Illinois, USA | [3]School For Engineering of Matter, Transport and Energy, Arizona State University, Tempe, Arizona, USA | [4]Department of Mechanical Engineering, Northwestern University, Evanston, Illinois, USA | [5]Department of Materials Science and Engineering, Northwestern University, Evanston, Illinois, USA | [6]Department of Biomedical Engineering, Northwestern University, Evanston, Illinois, USA | [7]Department of Neurological Surgery, Feinberg School of Medicine, Northwestern University, Chicago, Illinois, USA

Correspondence: Yonggang Huang (y-huang@northwestern.edu) | Haohui Zhang (haohui.zhang@northwestern.edu)

Received: 25 June 2025 | **Revised:** 11 May 2026 | **Accepted:** 14 May 2026

Keywords: biofluid flow rate | energy efficiency | flow rate sensitivity | thermal flow sensor | transient heating

ABSTRACT

Accurate measurement of biofluid flow rate is critical for clinical diagnostics and physiological monitoring, such as in cerebrospinal fluid shunt assessment and vascular blood flow evaluation. Thermal flow sensors, particularly hot-film and calorimetric types, are widely used in biomedical settings due to their broad dynamic range and long-term stability. However, their performance declines at high flow rates. To overcome this drawback, we propose a transient heating method that applies a short-duration thermal pulse and tracks the peak temperature response. This method, validated by experiments using artificial blood and vessels, significantly improves sensitivity to the flow rate change at high flow rates and reduces energy consumption. There exists an optimal heating time to maximize sensitivity to the flow rate. A contour plot of flow rate sensitivity vs. the heating time and flow rate is obtained to guide the selection of optimal heating time for different flow conditions.

1 | Introduction

Accurate measurement of biofluid flow rates is essential for clinical diagnostics and physiological monitoring. For example, assessing cerebrospinal fluid flow rate is a key indicator of shunt patency in the management of hydrocephalus [1–4]. Quantifying sweat rate provides valuable insights into thermoregulatory dysfunction and heat-related illnesses [5]. Blood flow monitoring, meanwhile, plays a critical role in evaluating both microvascular and macrovascular health in clinical and research settings [6–8].

Various techniques have been developed for flow rate measurement, including ultrasound [9], cantilever-based sensors [10], piezoelectric sensors [11], and magnetic devices [12]. Among these, thermal flow sensors have emerged as a preferred choice in biomedical applications due to their distinct advantages. First, microheaters and thermal sensors can be easily fabricated using micromachining technology, simplifying the overall manufacturing process. Second, the absence of moving parts ensures high stability and ease of operation. Third, thermal flow sensors feature low power consumption and high sensitivity at low flow rates, making them particularly suitable for miniaturized systems [13, 14]. These characteristics make thermal flow sensors particularly well-suited for monitoring in physiological environments, where mechanical durability and operational safety are critical.

Yuanting Wei, Shupeng Li, and Kyung Rok Pyun contributed equally to this work.

Among thermal flow sensing techniques, hot-film and calorimetric methods are the most widely employed due to their versatility and reliable performance [13, 15, 16]. The hot-film method utilizes a single integrated heater-sensor element, offering a compact and straightforward design. In contrast, the calorimetric method utilizes a central heater accompanied by upstream and downstream temperature sensors, enabling the detection of flow-induced thermal asymmetry. Both methods have been successfully adapted for a variety of biomedical applications [1, 2, 5, 6, 17, 18].

The main drawback of both methods lies in their reduced sensitivity at high flow rates (e.g., >0.05 m/s) [16, 19], where the measured temperature change tends to saturate. While increasing the heating power could enhance sensitivity, biomedical applications are constrained by a maximum permissible temperature, which limits the allowable heating power. Additionally, since temperature is measured at the steady state, reaching this condition can be time-consuming, especially in larger systems [19, 20], resulting in operational delays. Moreover, energy continues to be consumed even after the steady state is reached, leading to inefficiencies in energy usage [16].

To address these limitations, we propose a transient heating method that applies a short-duration heating pulse and monitors the resulting peak temperature response of the system. This method offers two key advantages. First, the use of short heating durations allows for the application of higher heating power without exceeding safety limits, significantly enhancing temperature sensitivity to the flow rate change, especially at high flow rates. Second, by predetermining the heating time, the method eliminates the need to wait for the system to reach the steady state, significantly shortening the experimental wait time while also reducing energy consumption and improving overall efficiency.

In this study, we apply the transient heating method to blood vessels with high blood flow rates (above 0.05 m/s), and optimize the heating power and heating time to significantly improve flow rate sensitivity over the existing methods [16, 19]. The proposed transient heating method is validated by our benchtop experiments using a silicone tube and blood-mimicking fluid (40% glycerol solution) as an artificial vessel and blood substitutes, respectively. A contour is presented to guide the selection of optimal heating time under various flow rates. This method enables precise and rapid measurements across a wide range of physiological conditions, making it highly practical for diverse biomedical applications.

2 | Theory for Flow Rate Measurement

Figure 1A shows a vessel containing blood. The vessel is idealized as an infinitely long cylinder oriented along the z-axis, with the inner and outer radii r_i and r_o, respectively. A thin, rectangular heat patch ($2r_o\Delta\theta$ times w), which can be modeled as a surface heating source, is wrapped to the external surface of the vessel, with the coordinates $r = r_o$, $-\Delta\theta < \theta < \Delta\theta$ and $-w/2 < z < w/2$ in the cylindrical coordinate system (r, θ, z).

The temperature rise in the vessel, after the heat patch is turned on, depends on the blood flow rate [7, 13, 14, 16, 19]. The established relation between the flow rate and the temperature rise at the sensor on the outer wall of the vessel forms the basis for determining the flow rate [1, 7, 19]. In existing methods [1, 7, 19], the heat patch remains on continuously, and the temperature is measured only after the system reaches a steady state. In contrast, we propose a new transient heating method in which the heat patch is turned off at a predetermined time τ (Figure 1B), and the peak temperature rise is recorded.

2.1 | Flow Velocity in the Vessel

Flow within the vessel is assumed to be fully developed, laminar, and Newtonian (Note S1 and Figure S1). The local velocity $u(r)$ at a radial position r is described by the Poiseuille solution for flow [21, 22]:

$$u(r) = 2\bar{u}\left(1 - \frac{r^2}{r_i^2}\right) \tag{1}$$

where $\bar{u}$ is the flow rate, i.e., the mean flow velocity of the fluid within the tube, and it is smaller than 1 m/s for blood flow [19, 23, 24]. Given that the dynamic viscosity of blood typically ranges from 3 to 6 mPa·s [25, 26], the corresponding maximum Reynolds number remains below 2300 [27] such that the assumption of laminar flow is valid throughout the analysis.

2.2 | Heat Equation in the Vessel and Blood

Heat transfer within the vessel is described by the heat conduction equation:

$$\frac{\partial T}{\partial t} - \alpha_s \nabla^2 T = 0 \tag{2}$$

where T is the temperature, and α_s denotes the thermal diffusivity of the vessel. Heat transfer within the blood is governed by [28]:

$$\frac{\partial T}{\partial t} + u\frac{\partial T}{\partial z} - \alpha_f \nabla^2 T = 0 \tag{3}$$

where α_f is the thermal diffusivity of the fluid (blood), and the velocity u is given in Equation (1). The initial temperature (at time $t = 0$) throughout both the vessel wall and the blood is set to the ambient environmental temperature T_0.

On the external surface of the vessel, heat exchange with the environment occurs through natural convection. Simultaneously, a heat patch is applied to this surface to deliver thermal energy. The boundary condition at the outer radius $r = r_o$ is:

$$k_s \frac{\partial T}{\partial r}\Big|_{r=r_o} = q(t) - h(T - T_0) \tag{4}$$

where k_s denotes the thermal conductivity of the vessel, h is the heat transfer coefficient between the vessel and the environment, and $q(t)$ is the heat flux delivered to the vessel by the heat patch, which is a non-zero constant q_0 only within the patch $-\Delta\theta < \theta < \Delta\theta$, $-w/2 < z < w/2$ and for the duration $0 < t < \tau$ (τ is the heating time, Figure 1B).

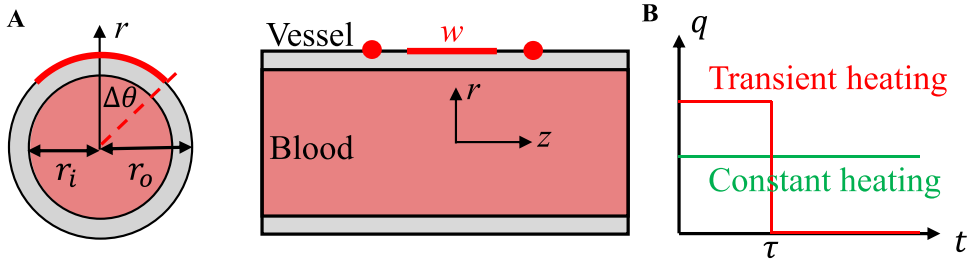

FIGURE 1 | (A) Schematic of the heat patch and thermal sensors (red dots) mounted on the external surface of the cylindrical vessel containing blood. The heat patch geometry is defined by its axial width w and angular span $\Delta\theta$. (B) Comparison between the existing constant heating method, which applies constant power continuously, and the proposed transient heating method, where heating stops at a predetermined heating time τ.

At the interface between the vessel and the blood, both temperature and heat flux are continuous:

$$T|_{r_i^+} = T|_{r_i^-} \tag{5}$$

$$k_s \frac{\partial T}{\partial r}|_{r_i^+} = k_f \frac{\partial T}{\partial r}|_{r_i^-} \tag{6}$$

where k_f denotes the thermal conductivity of the blood.

2.3 | Scaling Law

Given the governing equations along with the boundary and interface conditions, the temperature rise $\Delta T = T - T_0$ has the following dimensionless form, i.e., a scaling law:

$$\frac{k_f \Delta T}{q_0 r_i} = f_1\left(\frac{\alpha_f t}{r_i^2}, \frac{r}{r_i}, \theta, \frac{z}{r_i}, \frac{\alpha_s}{\alpha_f}, \frac{k_s}{k_f}, \frac{\bar{u} r_i}{\alpha_f}, \frac{r_o}{r_i}, \frac{h r_i}{k_f}, \frac{\alpha_f \tau}{r_i^2}, \frac{w}{r_i}, \Delta\theta\right) \tag{7}$$

where f_1 is a non-dimensional function. With blood flow, the maximum temperature rise in the vessel is always smaller than that without blood flow, as the moving blood carries away some heat. Without blood flow, the maximum temperature rise occurs at the center of the heat patch ($r = r_o, \theta = 0, z = 0$) at the end of heating $t = \tau$, i.e.:

$$\frac{k_f \Delta T_{max}}{q_0 r_i} = f_1\left(\frac{\alpha_f \tau}{r_i^2}, \frac{r_o}{r_i}, 0, 0, \frac{\alpha_s}{\alpha_f}, \frac{k_s}{k_f}, 0, \frac{r_o}{r_i}, \frac{h r_i}{k_f}, \frac{\alpha_f \tau}{r_i^2}, \frac{w}{r_i}, \Delta\theta\right) \tag{8}$$

The maximum allowed temperature rise ΔT_{max} depends on biomedical applications, for example, approximately 2 K for brain tissue [29, 30] and around 10 K for skin [31–33]. For a given maximum temperature rise ΔT_{max}, Equation (8) determines the maximum heat flux q_0 from the heat patch. This maximum q_0 increases as the heating time τ decreases (Figure 2E), enabling the use of much larger heat power over a short heating time, thereby enhancing the temperature change in the system and increasing the sensitivity of temperature response to the flow rate.

Two commonly used methods for determining flow rate based on temperature measurements are the hot-film and calorimetric methods [13–15]. In the hot-film method [19, 34], the sensor measures the steady-state temperature, averaged over the heat patch, at a given flow rate $\bar{u}$ and constant heating. We propose to use the hot-film method with transient heating (Figure 1B), and measure the peak temperature rise (with respect to time) averaged over the heat patch, denoted as $\Delta T_{peak,\,hot-film}$ or $\Delta T_{peak,h}$.

In the calorimetric method [5, 35, 36], the steady-state temperature difference between upstream and downstream sensors—placed symmetrically around the heat patch (Figure 1A)—is measured at a given flow rate $\bar{u}$ and constant heating. We propose to use the calorimetric method with transient heating and measure the peak temperature difference (with respect to time), denoted as $\Delta T_{peak,calorimetric}$ or $\Delta T_{peak,c}$.

These measured temperatures satisfy the following scaling law:

$$\frac{k_f \Delta T_{peak,j}}{q_0 r_i} = f_j\left(\frac{\alpha_s}{\alpha_f}, \frac{k_s}{k_f}, \frac{\bar{u} r_i}{\alpha_f}, \frac{r_o}{r_i}, \frac{h r_i}{k_f}, \frac{\alpha_f \tau}{r_i^2}, \frac{w}{r_i}, \Delta\theta\right) \tag{9}$$

or its ratio to Equation (8) yields,

$$\frac{\Delta T_{peak,j}}{\Delta T_{max}} = f_j'\left(\frac{\alpha_s}{\alpha_f}, \frac{k_s}{k_f}, \frac{\bar{u} r_i}{\alpha_f}, \frac{r_o}{r_i}, \frac{h r_i}{k_f}, \frac{\alpha_f \tau}{r_i^2}, \frac{w}{r_i}, \Delta\theta\right) \tag{10}$$

where the subscript j is either "hot-film" or "calorimetric", and both f_j and f_j' are non-dimensional functions.

3 | Results and Discussion

The baseline geometries and material properties are fixed as [19] $r_i = 2.975$ mm, $r_o = 3.325$ mm, $\alpha_s = 0.126$ mm^2/s and $k_s = 0.46$ W/(m K) for the vessel; $\alpha_f = 0.137$ mm^2/s and $k_f = 0.52$ W/(m K) for the blood; and $w = 60$ mm and angular width of 7.5 mm (corresponding to $\Delta\theta = 64.6°$) for the heat patch. The heat transfer coefficient is $h = 10$ W/(m^{2}K) [37]. The upstream and downstream sensors are positioned 2 mm [1, 6] away from the edges of the heat patch on either side. We focus on the effects of heating time τ and high flow rate $\bar{u}$ (> 0.05 m/s), and optimize the heating time to increase the flow rate sensitivity to $\Delta T_{peak,j}/\Delta T_{max}$.

3.1 | Transient Heating Method

Figure 2A shows the temperature distributions in the vessel and blood, obtained by COMSOL Multiphysics 6.2 for the flow rate $\bar{u} = 0.2$ m/s. For the constant heating method (Figure 2B), the temperature rise is low because the heating power is low in order

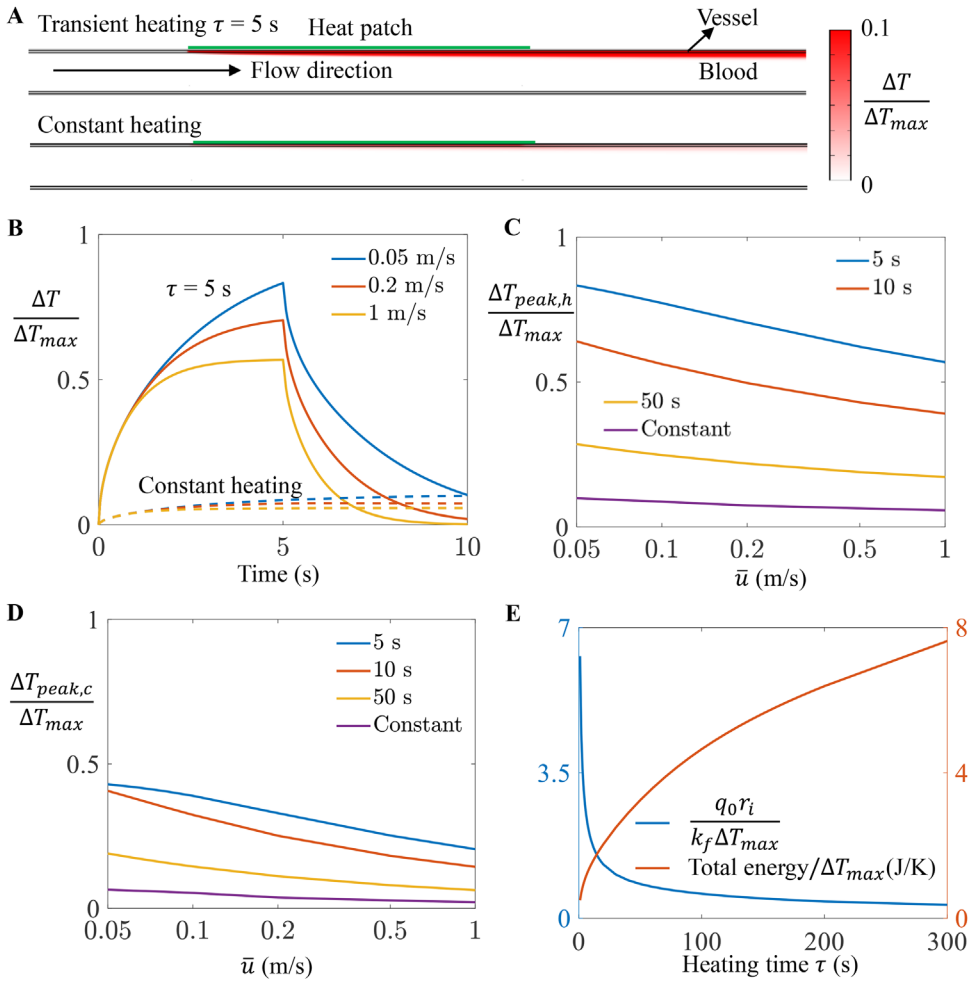

FIGURE 2 | (A) Temperature distributions at $t = 5$ s for transient heating with heating time $\tau = 5$ s and at steady state for constant heating, both at the flow rate $\bar{u} = 0.2$ m/s. (B) Evolution of sensor temperature rise (temperature rise averaged over the heat patch) at flow rate $\bar{u} = 0.05$, 0.2, and 1 m/s. (C, D) The peak temperature rise ($\Delta T_{peak,h}$ in C and $\Delta T_{peak,c}$ in D) vs. the flow rate $\bar{u}$ for heating time $\tau = 5$, 10, and 50 s, and constant heating. (E) Normalized heat flux delivered to the vessel $\frac{q_0 r_i}{k_f \Delta T_{max}}$, and total energy delivered to the vessel per heating cycle (normalized by ΔT_{max}) as a function of heating time τ.

not to exceed the maximum allowed temperature rise, yielding low sensitivity at high flow rates. On the contrary, for transient heating with heating time $\tau = 5$ s (Figure 2A), the temperature rise is significantly higher, especially around the heat patch. This is because transient heating allows the use of significantly higher heat power without exceeding the maximum allowed temperature rise, leading to much improved sensitivity.

Figure 2B depicts the temperature rise of the sensor (i.e., averaged over the heat patch in the hot-film method) vs. time. It reaches the peak at the end of heating $t = \tau$. This peak is shown vs. the flow rate $\bar{u}$ in Figure 2C for the heating time $\tau = 5$, 10, and 50 s and constant heating, providing the basis for determining the flow rate from the measured peak temperature rise. For a short heating time τ, $\Delta T_{peak,h}/\Delta T_{max}$ approaches 1 as most of the heat remains localized near the heat patch. As the heating time τ increases, thermal diffusion spreads the heat into the surrounding vessel and blood, thereby reducing $\Delta T_{peak,h}/\Delta T_{max}$.

The slope of $\Delta T_{peak,h}$ with respect to flow rate gives the sensitivity. At the high flow rate $\bar{u} = 1$ m/s, the slopes for $\tau = 5$ and 10 s are ~10 times larger than the slope for the constant heating method. For a representative thermistor used in bioflow sensing, the reported temperature resolution is between 0.01 and 0.07 K [6, 7, 35]. For $\Delta T_{max} = 2$ K as for brain tissue [29, 30] and temperature sensing resolution of 0.04 K, the transient heating method can detect a 30% change in blood flow rate around $\bar{u} = 1$ m/s. In contrast, the constant heating method would require a 290% change in flow rate to be detectable. For temperature sensing resolution of 0.01 K, the transient heating and constant heating methods can detect 7.5% and 72% change in flow rate, respectively. As an example, the proposed transient heating method enables sensitive detection of flow velocity changes within the clinically relevant ICA/CCA (internal carotid artery/ common carotid artery) PSV (peak systolic velocity) ratio range (≥2.0) [38]. This range corresponds to ≥50% stenosis, and it is difficult to detect using the constant heating method. Although Doppler ultrasound remains the gold standard, it is primarily a snapshot-based modality that requires professional operation and bulky instrumentation. In contrast, our transient heating method provides a complementary, long-term monitoring framework. It is specifically designed to detect the same velocity-based criteria defined by clinical

standards, but with the added benefits of autonomous operation, ultra-low cost, and a flexible form factor suitable for continuous wearable or implantable use.

Similarly, for the calorimetric method, the sensitivity for $\tau = 5$ s is also significantly higher than that of the constant heating method (Figure 2D).

Figure 2E gives the total energy consumed during a heating cycle, $2wr_0\Delta\theta q_0\tau$, normalized by ΔT_{max}, vs. the heating time τ. The energy consumption for the proposed transient heating (e.g., $\tau =$ 5 s) is only 1/7 of that for constant heating (e.g., $\tau = 400$ s in prior experiments [19]), i.e., energy efficient.

In addition, with various vessel diameters (Figure S2) and heat transfer coefficients (Figure S3), the proposed transient heating method maintains superior sensitivity compared with the constant heating approach. This method also exhibits stronger robustness against temperature fluctuations (Note S2 and Figure S4).

3.2 | Flow Rate Sensitivity

We studied heating times ranging from 1 to 130 s (additional results are provided in Figure S5). Based on the contour plots of $\Delta T_{peak,h}/\Delta T_{max}$ and $\Delta T_{peak,c}/\Delta T_{max}$ vs. the flow rate and heating time in Figure 3A,B, we obtain the flow rate sensitivity in Figure 3C,D for the hot-film and calorimetric methods, respectively, where the flow rate sensitivity S_j is defined as:

$$S_j = \frac{\mathrm{d}\left(\Delta T_{peak,j}/\Delta T_{max}\right)}{\mathrm{d}\ln\left(\bar{u}r_i/\alpha_f\right)} \tag{11}$$

to quantify how $\Delta T_{peak,j}/\Delta T_{max}$ changes with respect to the normalized flow rate, $\bar{u}r_i/\alpha_f$. For each given flow rate, the sensitivity reaches a maximum at an optimal heating time given in Figure 3E. The sensitivity at this optimal heating time is given in Figure 3F, which clearly shows that the optimized transient heating method gives much higher sensitivity than the constant heating method. For example, a typical physiological flow rate of 800 mL/min [19] corresponds to a dimensionless value of $\bar{u}r_i/\ \alpha_f = 1.0 \times 10^4$, where a heating time of 4.9 s yields a sensitivity that is 5 times greater than that of the constant heating method.

The optimal heating time depends on the vessel radius (Figure S6) and the heat-transfer coefficient (Figure S7); however, the transient heating method consistently achieves higher sensitivity than the constant heating method under all examined conditions.

3.3 | Experimental Validation

To evaluate the physiological relevance of the proposed transient heating method, we established a bio-mimetic experimental setup utilizing viscosity-matched blood-mimicking fluid (a 40% glycerol solution) [39, 40] and a soft silicone tube to replicate the rheological and mechanical properties of the human cardiovascular environment (Figure 4A). Furthermore, while the peristaltic pump utilized in our experiments introduces inherent flow pulsatility, paralleling physiological hemodynamics, we observed that the peak temperature response remains highly robust against these temporal oscillations. The material properties are $\alpha_s = 0.106$ mm^2/s and $k_s = 0.15$ W/(m K) for the silicone rubber tube [41]; α_f $= 0.124$ mm^2/s and $k_f = 0.45$ W/(m K) for the 40% glycerol solution [42]. Slightly different from the baseline values, the inner and outer diameters of the tube are r_i 4.76 mm (3/16″) and r_o 6.35 mm (1/4″), and the heat patch has width $w = 60$ mm and angular width 7.5 mm. In order to maintain a representative value $\Delta T_{max} = 5$ K for the maximum allowed temperature rise at zero flow rate, the total heat power of the heat patch for the constant heating method is 0.117 W, while that for the transient heating method with heating time $\tau = 20$ s is substantially higher, 0.407 W. Here, the heat power is the product of the heat flux q_0 and the area of the heat patch.

A negative-temperature-coefficient (NTC) thermistor is attached to the center of the heater to record the local temperature. Additional NTC thermistors are attached upstream and downstream of the heater, positioned 2 mm from the heater edge, and are used as sensors for the calorimetric method. Similar to prior measurements [43, 44], the encapsulation of the NTC thermistor induces thermal resistance at its interface with the tube, which is determined as 0.01 m^{2}K/W by fitting the steady temperature of experiments for constant heating and 0.05 m/s flow rate (Figure 4B). This thermal resistance 0.01 m^{2}K/W, which is on the same order of magnitude as the literature values [19], also yields good agreements with the constant heating experiments at other flow rates (Figure 4B), as well as with the transient heating experiments with heating time $\tau = 20$ s (Figure 4C) without any additional fitting. Then, fitting the time evolution of the temperature at 20 s gives the heat transfer coefficient $h =$ 25 W/(m^{2}K).

The significant performance enhancement of the transient heating method over the conventional constant heating method is validated in Figure 4D,E. The experimental data exhibit excellent agreement with numerical simulations. Specifically, for the hot-film configuration, the transient method yields a temperature response of 0.47 K across the range of high flow rate (0.05–1 m/s), a threefold increase compared to the 0.16 K observed under constant heating. Similarly, for the calorimetric method, the temperature differential $\Delta T_{peak,c}$ within the same high-flow range shows a comparable threefold enhancement over the constant heating baseline. These results collectively verify that the proposed transient heating method significantly extends the dynamic range of thermal sensors, enabling precise measurement at high flow rates that were previously challenging to resolve.

A cooling period is required to restore the baseline temperature between heating pulses. Simulations show that a 10 s cooling time is sufficient for heating durations of 1–130 s, with less than 2% variation in peak temperature after five consecutive cycles (Figure S8). Thus, the method enables stable repeated measurements, with a representative sampling frequency of about 0.05 Hz for a 10 s heating time. This cooling period was further validated experimentally: using a 10 s cooling interval followed by a 50 s heating duration for five consecutive cycles, both the hot-film and calorimetric methods demonstrated peak temperature consistency with a deviation of less than 2.5% across cycles (Figure 4F).

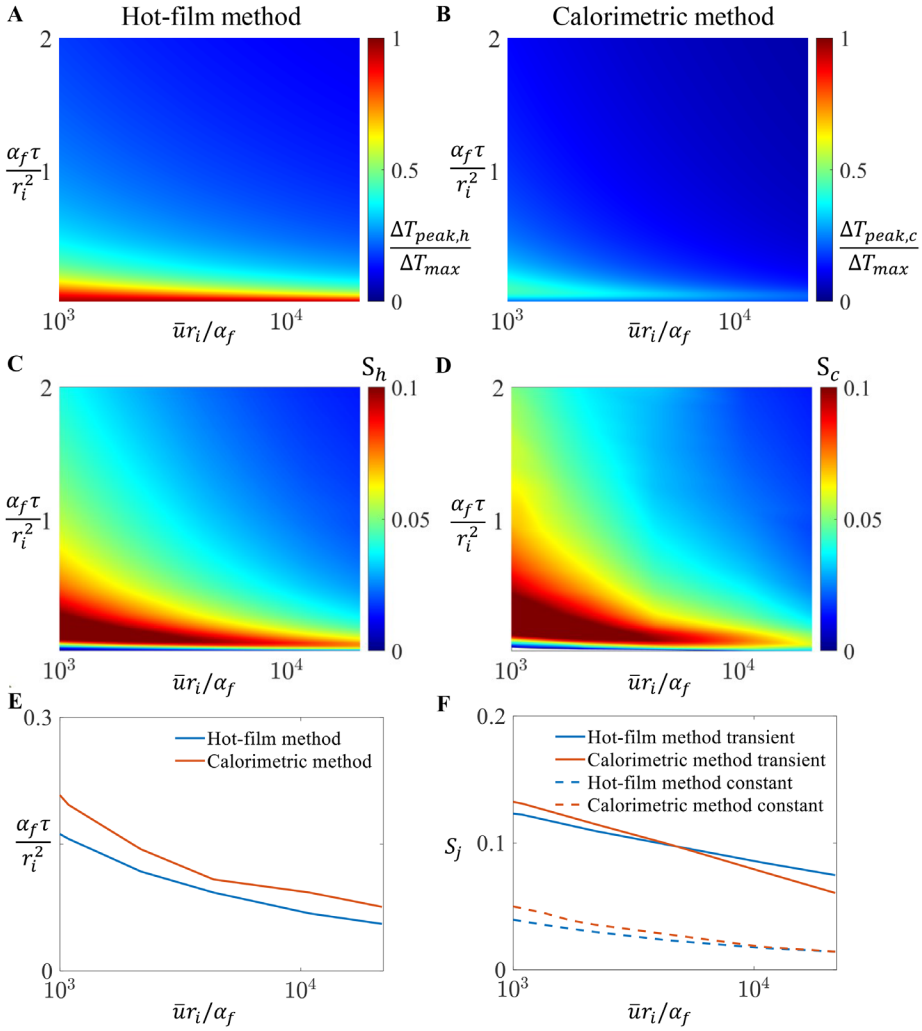

FIGURE 3 | Contour plots of the (A) normalized peak temperature rise averaged over the heat patch, $\Delta T_{peak,h}/\Delta T_{max}$, (B) normalized peak temperature difference between upstream and downstream sensors, $\Delta T_{peak,c}/\Delta T_{max}$, (C) sensitivity S_h for the hot-film method, (D) sensitivity S_c for the calorimetric method, vs. the heating time and flow rate. (E) Optimal heating time to maximize sensitivity vs. the flow rate. (F) Comparison of sensitivity between the constant and optimized transient heating methods.

Furthermore, the long-term operational stability of the device was evaluated over a 5-day continuous testing period. The peak temperature response remained remarkably consistent, with a total variation of less than 0.1K throughout the 5-day duration (Figure 4G). This high degree of repeatability, combined with the absence of significant signal drift, confirms the robustness of the transient heating sensing platform and its suitability for sustained, long-term flow monitoring applications.

Besides the current experimental setup, the proposed transient heating strategy can be readily integrated into existing biocompatible implantable sensor systems by simply modifying the heating protocol, without altering the material composition or device structure.

4 | Conclusions

We apply transient heating to the hot-film and calorimetric methods in this paper in order to measure high blood flow rates in vessels, with potential applicability to a broad range of biofluid flow sensing. Unlike conventional constant heating, our method turns off the heat patch at a predetermined heating time and captures the peak temperature response, allowing for maximizing sensitivity tailored to different flow rates. It achieves significantly improved sensitivity—particularly at high flow rates where the existing methods often struggle—because the heating power can be substantially increased without exceeding thermal safety limits. Additionally, it reduces energy consumption substantially, making the method more efficient and potentially more suitable for integration into wearable or implantable medical devices. Overall, the proposed strategy offers a promising pathway for high-resolution, low-power flow sensing in both clinical diagnostics and physiological monitoring.

5 | Experimental Section/Methods

5.1 | Fabrication of Electronics

To enhance sensing accuracy through efficient thermal transfer and ensure conformal contact with the curvilinear surface

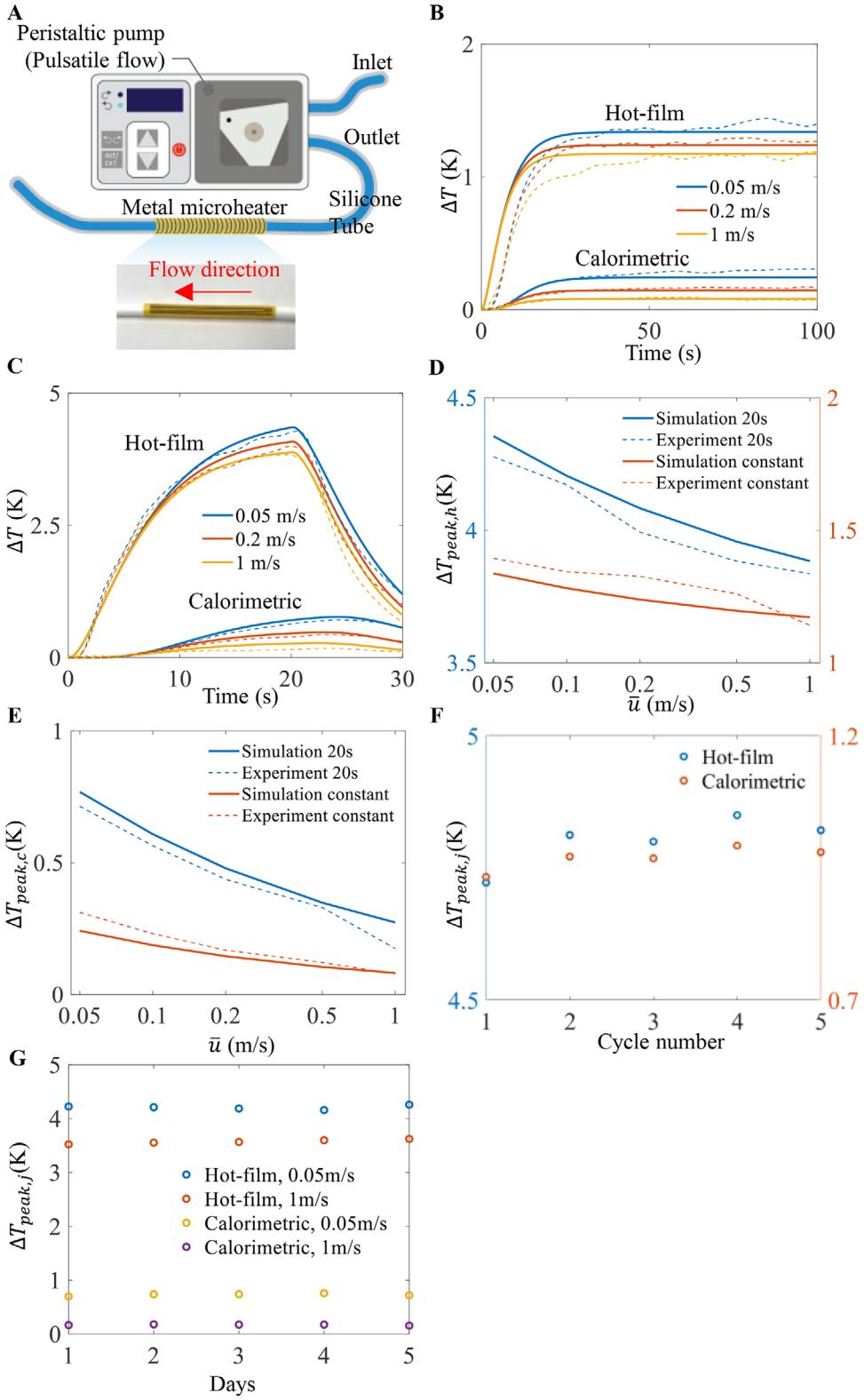

FIGURE 4 | (A) Experimental setup. (B) Evolution of sensor temperature rise using the constant heating method (Solid lines represent simulation results, while dashed lines represent experimental results). (C) Evolution of sensor temperature rise using the transient heating method ($\tau = 20$ s). (D) Comparison of peak temperature rise of the sensor vs. the flow rate for the transient heating method with heating time $\tau = 20$ s, and constant heating methods, validating the sensitivity enhancement in the hot-film method. (E) Sensitivity comparison for the calorimetric method. (F) Experimental validation of $\Delta T_{peak,j}$ invariance across five consecutive heating–cooling cycles. (G) Stability of the device over 5 days, showing consistent peak temperature response for both hot-film and calorimetric methods across two flow rates.

of the tube, a flexible printed circuit board (fPCB) is fabricated using a thin copper/polyimide (PI)/copper laminate (AP8535R, Pyralux, DuPont) with respective thicknesses of 18, 75, and 18 μm. A UV laser cutter (ProtoLaser U4, LPKF) is employed to ablate the copper layers and define the conductive traces and bond pads. For component assembly, solder paste (TS391LT, Chip Quik) is applied, and reflow soldering is performed using a heat gun (AOYUE Int866). For temperature measurement, the circuit was configured as a Wheatstone bridge [45], with NTC thermistors (NCP03XH103F05RL, Murata Electronics) positioned at the center of the heater and along the flow direction, and an additional reference NTC thermistor placed at a location isolated from the fluid flow to capture environmental temperature variations. The differential signals from the bridge were amplified using instrumentation amplifiers (INA333AIDRGR, Texas Instruments) to suppress common-mode environmental temperature variations and improve measurement accuracy. The amplified signals were acquired using an external data acquisition system (Arduino Mega 2560, Arduino).

5.2 | Fabrication of Heater

A 12.5 μm-thick PI film is attached onto a glass slide coated with polydimethylsiloxane. A metal microheater is formed onto the PI film by depositing a layer of Cr/Au metal using an e-beam evaporator, followed by a process of photolithography and wet etching to create a 200 μm-wide serpentine metal pattern. The patterned metal layer is encapsulated by spin-coating a PI precursor at 3000 rpm, then baked at 150°C for 10 min and at 265°C in a vacuum oven to form a 1.5 μm-thick PI layer. A copper mask is aligned on top of the heater for contact pad patterning, followed by photolithography and wet etching to make the contact pads. After removing the Cu mask layer using wet etching, the UV laser cutter is used for the border outline.

5.3 | Benchtop Study

Flow-controlled experiments are conducted at flow rates of 0, 0.05, 0.1, 0.2, 0.5, and 1 m/s, using a peristaltic pump (GP 1000, Fisher Scientific). Both the NTC thermistor and the heater are mounted on the top surface of a soft silicone tube (5296N13, McMaster-Carr, inner diameter of 4.76 mm (3/16″) and outer diameter of 6.35 mm (1/4″)) using double-sided medical silicone tape (2477P, 3 M) to ensure stable contact. The working fluid was a 40% glycerol solution (G5516, Sigma-Aldrich) to mimic the viscosity of blood. Furthermore, to minimize convective heat loss and ensure thermal insulation, the NTC thermistor is encapsulated using an acrylic foam insulation tape (4950 VHB, 3 M). Electrical power is supplied to the heater using a low-noise precision AC/DC current source (Keithley 6221). For the hot-film method, an NTC thermistor was placed at the center of the heater, while for the calorimetric method, NTC thermistors were positioned 2 mm upstream and 2 mm downstream from the heater along the flow direction.

Funding

This work was supported by the Querrey-Simpson Institute for Bioelectronics at Northwestern University

Conflicts of Interest

The authors declare no conflicts of interest.

Data Availability Statement

The data that support the findings of this study are available from the corresponding author upon reasonable request.

References

1. S. R. Krishnan, H. M. Arafa, K. Kwon, et al., "Continuous, Noninvasive Wireless Monitoring of Flow of Cerebrospinal Fluid Through Shunts in Patients With Hydrocephalus," *NPJ Digital Medicine* 3, no. 1 (2020): 29, https://doi.org/10.1038/s41746-020-0239-1.

2. S. R. Krishnan, T. R. Ray, A. B. Ayer, et al., "Epidermal Electronics For Noninvasive, Wireless, Quantitative Assessment of Ventricular Shunt Function in Patients With Hydrocephalus," *Science Translational Medicine* 10, no. 465 (2018): aat8437, https://doi.org/10.1126/scitranslmed.aat8437.

3. A. A. Linninger, M. Xenos, D. C. Zhu, M. R. Somayaji, S. Kondapalli, and R. D. Penn, "Cerebrospinal Fluid Flow in The Normal And Hydrocephalic Human Brain," *IEEE Transactions on Biomedical Engineering* 54, no. 2 (2007): 291–302, https://doi.org/10.1109/TBME.2006.886853.

4. B. J. Kim, W. Jin, A. Baldwin, et al., "Parylene MEMS Patency Sensor for Assessment of Hydrocephalus Shunt Obstruction," *Biomedical Microdevices* 18 (2016): 1–13, https://doi.org/10.1007/s10544-016-0112-9.

5. K. Kwon, J. U. Kim, Y. Deng, et al., "An On-Skin Platform for Wireless Monitoring of Flow Rate, Cumulative Loss and Temperature of Sweat in Real Time," *Nature Electronics* 4, no. 4 (2021): 302–312, https://doi.org/10.1038/s41928-021-00556-2.

6. R. C. Webb, Y. Ma, S. Krishnan, et al., "Epidermal Devices for Noninvasive, Precise, and Continuous Mapping of Macrovascular and Microvascular Blood Flow," *Science Advances* 1, no. 9 (2015): 1500701, https://doi.org/10.1126/sciadv.1500701.

7. D. Lu, S. Li, Q. Yang, et al., "Implantable, Wireless, Self-Fixing Thermal Sensors for Continuous Measurements of Microvascular Blood Flow in Flaps and Organ Grafts," *Biosensors and Bioelectronics* 206 (2022): 114145, https://doi.org/10.1016/j.bios.2022.114145.

8. Y. Tian, K. Yang, Y. Wang, et al., "Self-Adaptive Epidermal Blood Flow Sensor for High-Flux Vascular Access Monitoring of Hemodialysis Patients," *npj Flexible Electronics* 8, no. 1 (2024): 62, https://doi.org/10.1038/s41528-024-00342-y.

9. D. Vilkomerson and T. Chilipka, "Implantable Doppler System for Self-Monitoring Vascular Grafts," in IEEE Ultrasonics Symposium (IEEE, 2004), https://doi.org/10.1109/ULTSYM.2004.1417762.

10. K. Kwon, J. U. Kim, S. M. Won, et al., "A Battery-Less Wireless Implant for The Continuous Monitoring of Vascular Pressure, Flow Rate and Temperature," *Nature Biomedical Engineering* 7, no. 10 (2023): 1215–1228, https://doi.org/10.1038/s41551-023-01022-4.

11. L. Natta, V. M. Mastronardi, F. Guido, et al., "Soft and Flexible Piezoelectric Smart Patch for Vascular Graft Monitoring Based On Aluminum Nitride Thin Film," *Scientific Reports* 9, no. 1 (2019): 8392, https://doi.org/10.1038/s41598-019-44784-1.

12. B. Vennemann, D. Obrist, and T. Rösgen, "A Smartphone-Enabled Wireless and Batteryless Implantable Blood Flow Sensor for Remote

Monitoring of Prosthetic Heart Valve Function," *PLoS One* 15, no. 1 (2020): 0227372, https://doi.org/10.1371/journal.pone.0227372.

13. J. T. Kuo, L. Yu, and E. Meng, "Micromachined Thermal Flow Sensors—A Review," *Micromachines* 3, no. 3 (2012): 550–573, https://doi.org/10.3390/mi3030550.

14. S. Silvestri and E. Schena, "Micromachined Flow Sensors in Biomedical Applications," *Micromachines* 3, no. 2 (2012): 225–243, https://doi.org/10.3390/mi3020225.

15. N. Nguyen, "Micromachined Flow Sensors—A Review," *Flow measurement and Instrumentation* 8, no. 1 (1997): 7–16, https://doi.org/10.1016/S0955-5986(97)00019-8.

16. C. Cavaniol, W. Cesar, S. Descroix, and J.-L. Viovy, "Flowmetering for Microfluidics," *Lab on a Chip* 22, no. 19 (2022): 3603–3617, https://doi.org/10.1039/D2LC00188H.

17. P. Jiang, S. Zhao, and R. Zhu, "Smart Sensing Strip Using Monolithically Integrated Flexible Flow Sensor for Noninvasively Monitoring Respiratory Flow," *Sensors* 15, no. 12 (2015): 31738–31750, https://doi.org/10.3390/s151229881.

18. T. Jiang, L. Deng, W. Qiu, et al., "Wearable Breath Monitoring Via A Hot-Film/Calorimetric Airflow Sensing System," *Biosensors and Bioelectronics* 163 (2020): 112288, https://doi.org/10.1016/j.bios.2020.112288.

19. Y. Deng, H. M. Arafa, T. Yang, et al., "A Soft Thermal Sensor for The Continuous Assessment of Flow in Vascular Access," *Nature Communications* 16, no. 1 (2025): 38, https://doi.org/10.1038/s41467-024-54942-3.

20. V. Balakrishnan, T. Dinh, H.-P. Phan, D. V. Dao, and N.-T. Nguyen, "Highly Sensitive 3C-SiC on Glass Based Thermal Flow Sensor Realized Using MEMS Technology," *Sensors and Actuators A: Physical* 279 (2018): 293–305, https://doi.org/10.1016/j.sna.2018.06.025.

21. B. J. Kirby, *Micro-and Nanoscale Fluid Mechanics: Transport in Microfluidic Devices* (Cambridge University Press, 2010).

22. H. Bruus, *Theoretical Microfluidics* (Oxford University Press, 2007).

23. Y. C. Fung, *Biomechanics: Circulation* (Springer Science & Business Media, 2013).

24. D. N. Ku, "Blood Flow in Arteries," *Annual Review of Fluid Mechanics* 29, no. 1 (1997): 399–434, https://doi.org/10.1146/annurev.fluid.29.1.399.

25. R. S. Rosenson, A. Mccormick, and E. F. Uretz, "Distribution of Blood Viscosity Values and Biochemical Correlates in Healthy Adults," *Clinical Chemistry* 42, no. 8 (1996): 1189–1195, https://doi.org/10.1093/clinchem/42.8.1189.

26. E. Nader, S. Skinner, M. Romana, et al., "Blood Rheology: Key Parameters, Impact On Blood Flow, Role in Sickle Cell Disease and Effects of Exercise," *Frontiers in Physiology* 10 (2019): 1329, https://doi.org/10.3389/fphys.2019.01329.

27. T. L. Bergman, *Fundamentals of Heat and Mass Transfer* (John Wiley & Sons, 2011).

28. R. B. Bird, "Transport Phenomena," *Applied Mechanics Reviews* 55, no. 1 (2002): R1–R4, https://doi.org/10.1115/1.1424298.

29. H. Wang, B. Wang, K. P. Normoyle, et al., "Brain Temperature and Its Fundamental Properties: A Review for Clinical Neuroscientists," *Frontiers in Neuroscience* 8 (2014): 307, https://doi.org/10.3389/fnins.2014.00307.

30. E. A. Kiyatkin, "Brain Temperature Homeostasis: Physiological Fluctuations and Pathological Shifts," *Frontiers in Bioscience* 15 (2010): 73, https://doi.org/10.2741/3608.

31. D. G. Greenhalgh, M. B. Lawless, B. B. Chew, W. A. Crone, M. E. Fein, and T. L. Palmieri, "Temperature Threshold for Burn Injury: An Oximeter Safety Study," *The Journal of Burn Care & Rehabilitation* 25, no. 5 (2004): 411–415, https://doi.org/10.1097/01.BCR.0000138295.63830.90.

32. R. Landsberg, A. DeRowe, A. Katzir, A. Shtabsky, D. M. Fliss, and Z. Gil, "Laser-Induced Hyperthermia for Treatment of Granulation Tissue Growth in Rats," *Otolaryngology–Head and Neck Surgery* 140, no. 4 (2009): 480–486, https://doi.org/10.1016/j.otohns.2008.12.004.

33. M. W. Dewhirst, B. L. Viglianti, M. Lora-Michiels, M. Hanson, and P. J. Hoopes, "Basic Principles of Thermal Dosimetry and Thermal Thresholds for Tissue Damage From Hyperthermia," *International Journal of Hyperthermia* 19, no. 3 (2003): 267–294, https://doi.org/10.1080/0265673031000119006.

34. S. Wu, Q. Lin, Y. Yuen, and Y.-C. Tai, "MEMS Flow Sensors for Nano-Fluidic Applications," *Sensors and Actuators A: Physical* 89, no. 1-2 (2001): 152–158, https://doi.org/10.1016/S0924-4247(00)00541-0.

35. C. Hoera, M. M. Skadell, S. A. Pfeiffer, et al., "A Chip-Integrated Highly Variable Thermal Flow Rate Sensor," *Sensors and Actuators B: Chemical* 225 (2016): 42–49, https://doi.org/10.1016/j.snb.2015.11.009.

36. A. Rasmussen, C. Mavriplis, M. E. Zaghloul, O. Mikulchenko, and K. Mayaram, "Simulation and Optimization of A Microfluidic Flow Sensor," *Sensors and Actuators A: Physical* 88, no. 2 (2001): 121–132, https://doi.org/10.1016/S0924-4247(00)00503-3.

37. L. Zhang, Y. Zhong, X. Li, et al., "Effect of Twist Angle On Interfacial Thermal Transport in Two-Dimensional Bilayers," *Nano Letters* 23, no. 17 (2023): 7790–7796, https://doi.org/10.1021/acs.nanolett.3c01050.

38. E. G. Grant, C. B. Benson, G. L. Moneta, et al., "Carotid Artery Stenosis: Gray-Scale and Doppler US Diagnosis—Society of Radiologists in Ultrasound Consensus Conference," *Radiology* 229, no. 2 (2003): 340–346, https://doi.org/10.1148/radiol.2292030516.

39. M. Y. Yousif, D. W. Holdsworth, and T. L. Poepping, "A Blood-Mimicking Fluid for Particle Image Velocimetry With Silicone Vascular Models," *Experiments in Fluids* 50 (2011): 769–774, https://doi.org/10.1007/s00348-010-0958-1.

40. M. Y. Yousif, D. W. Holdsworth, and T. L. Poepping, "Deriving A Blood-Mimicking Fluid for Particle Image Velocimetry in Sylgard-184 Vascular Models," in 2009 Annual International Conference of the IEEE Engineering in Medicine and Biology Society (IEEE, 2009), 1412–1415, https://doi.org/10.1109/IEMBS.2009.5334175.

41. Y. Yang, M. Wu, A. Vázquez-Guardado, et al., "Wireless Multilateral Devices for Optogenetic Studies of Individual and Social Behaviors," *Nature Neuroscience* 24, no. 7 (2021): 1035–1045, https://doi.org/10.1038/s41593-021-00849-x.

42. Glycerine Producers' Association "*Physical Properties of Glycerine and Its Solutions*," (Glycerine Producers' Association, 1963), 5.

43. S. Li, D. Lu, M. Pet, J. A. Rogers, and Y. Huang, "An Analytical Model for Sensing Microvascular Blood Flow in Flaps and Organ Grafts," *Journal of the Mechanics and Physics of Solids* 170 (2023): 105119, https://doi.org/10.1016/j.jmps.2022.105119.

44. L. Qiu, Y. Ouyang, Y. Feng, X. Zhang, and X. Wang, "In Vivo Skin Thermophysical Property Testing Technology Using Flexible Thermosensor-Based 3ω Method," *International Journal of Heat and Mass Transfer* 163 (2020): 120550, https://doi.org/10.1016/j.ijheatmasstransfer.2020.120550.

45. K. Kwon, J. U. Kim, Y. Deng, et al., "An On-Skin Platform For Wireless Monitoring of Flow Rate, Cumulative Loss and Temperature of Sweat in Real Time," *Nature Electronics* 4, no. 4 (2021): 302–312, https://doi.org/10.1038/s41928-021-00556-2.

Supporting Information

Additional supporting information can be found online in the Supporting Information section.

Supporting File: adfm75992-sup-0001-SuppMat.docx.